Astron. Astrophys. 179, 41–59 (1987)

ASTRONOMY
AND
ASTROPHYSICS

VLA high resolution observations of weak Leiden-Berkeley Deep-Survey (LBDS) sources

M.J.A. Oort[1], P. Katgert[1], F.W.M. Steeman[1] and R.A. Windhorst[2]

[1] Sterrewacht Leiden, Postbus 9513, 2300 RA Leiden, The Netherlands
[2] Mount Wilson and Las Campanas Observatories, Pasadena, CA 91101, USA

Received September 24, accepted December 2, 1986

Summary. We present high resolution (1″) snapshot maps of 133 radio sources from the Leiden-Berkeley Deep Survey (LBDS), made with the VLA in the A-configuration. The large majority of these sources have flux densities between 1 and 100 mJy at 1.4 GHz, the median flux density of the present sample is 5 mJy.

A subsample of 85 of these sources forms a representative subset of the complete, optically identified ($m_F - \lim \approx 22^{\mathrm{m}}.5$) LBDS sample. This subsample allows the first unbiased study of the morphology of radio galaxies at these low flux densities. An additional 37 sources from the LBDS for which no optical identification could previously be found, have also been mapped to allow identification attempts on very deep optical material.

Combining all radio-morphological data now available for the LBDS, we find that the median angular size of a complete radio sample decreases with decreasing flux density, to as low a value as $\sim 2''$ between 1 and 10 mJy. This result is probably due to a combination of a changing composition of the radio galaxy population and a general decrease of intrinsic sizes of radio sources towards lower radio luminosities.

A comparison of the angular sizes of the classical *red* (elliptical) radio galaxies with those of the *blue* radio galaxies that become increasingly dominant in the 1–10 mJy range, show the latter to be significantly smaller than the former. While 10% of the red galaxies are not resolved by the 1″.4 beam, 50% of the blue radio galaxies remain unresolved. Although most of the red mJy radio galaxies are resolved, their intrinsic sizes seldom exceed 100–200 kpc, and their median intrinsic size is about 50 kpc ($H_0 = 50\,\mathrm{km\,s^{-1}\,Mpc^{-1}}$). The present data for the red radio galaxies seem to support that – at least for the intermediate to low radio luminosities – a dependence of intrinsic size on radio luminosity, similar to the one found by Gavazzi and Perola (1978) is present at higher redshifts as well.

We find definite indications for a decrease of intrinsic size with increasing redshift, with a relation that results in a decrease of a factor 4 in size at $z = 0.5$ with respect to the local value at the same radio power.

The large increase in radio resolution, and hence positional accuracy, shows the overall contamination of the optical identifications based on the WSRT positions to have been estimated correctly. However, the contamination fraction appears to be strongly dependent on optical type and color.

Key words: radio sources – radio galaxies: evolution of – structure of

1. Introduction

Several systematic deep surveys of extragalactic radio sources have been made with the Westerbork Synthesis Radio Telescope (WSRT) over the last 15 years. Most recently, two surveys of comparable sensitivity and statistical weight were made at 1.4 GHz, namely one of several selected areas for which deep Mayall 4m plate material was available (Windhorst et al., 1984), and one of several survey areas in the Einstein deep survey program (Katgert-Merkelijn et al; 1985).

The combination of the former Westerbork radio data with the deep 4-color Mayall plates has become known as the Leiden-Berkeley Deep Survey (LBDS) and has been discussed in a series of papers (Windhorst et al., 1984 Kron et al., 1985 Windhorst; 1984). The survey contains 306 radio sources above flux density limits of between 0.6 and 1.4 mJy. The median flux in the sample is ~ 6 mJy. The radio beam has halfwidths of 12″ by 12″/sin δ, resulting in positional accuracies of a few tenths of an arcsecond to, at most, a few arcseconds.

The optical material consists of 4m Mayall photometric plates in four colors (U, J, F and *N*) reaching limiting magnitudes of 23.5 (*U* and *J*), 22.5 (*F*), and 21.0 (*N*). Optical identifications on the basis of positional coincidence alone yielded 146 candidates, while 25 other sources were considered reliably identified (these were mostly clearly resolved radio sources).

Because of its flux range, the LBDS is very well suited for a study of the intermediate-to-low radio luminosity radio galaxies out to considerable redshifts (i.e. well beyond unity). The optical limits result in maximum redshifts of between 0.5 and 1.0 for the various classes of radio galaxies that populate this flux range.

Some of the major results of the LBDS were to define the various radio galaxy classes and to provide estimates of their space densities over the accessible redshift range. On the basis

Send offprint requests to: M.J.A. Oort of optical colors and radio morphology, two radio galaxy classes were defined. The first one has the optical colors of the classical elliptical ("red") radio galaxies found in abundance at higher radio fluxes. The second one has bluer colors and a more extended optical morphology than the first one and could be thought to consist entirely of normal spirals *if it were not for the frequently unusually large radio luminosities.*

In this paper we present high resolution radio observations with the Very Large Array (VLA) at 20 cm of a large, representative subset of the optically identified LBDS radio sources, as well as of a smaller subset of LBDS "empty fields" (the latter to allow optical identification on very deep CCD exposures, see Windhorst et al., 1986).

Similar morphology studies have been carried out earlier with the VLA (e.g. Fielden et al; 1983 and Lawrence et al; 1984), but down to flux levels which are 10–100 times as bright as ours.

The data presented in this paper were obtained during two runs, more than one year apart. Together with the WSRT data of sources for which the WSRT resolution was adequate, we now have information required for a discussion of the angular size distribution of a complete source sample between 1 and 50 mJy. Combined with angular size distributions at higher flux levels, we can study the flux density dependence of the distribution, and the median angular size, $\psi_{\rm med}$. The present data also allow us to study possible morphological differences between the various classes of radio galaxy, as well as correlations between morphology and redshift or radio luminosity.

2. Observations and reduction

2.1. Observations

The snapshot observations were made with the VLA [for a detailed description of the VLA see Thompson et al. (1980)] in the A configuration (minimum baseline: 0.8 km, maximum baseline: 36.6 km) in two periods of 24 hours each, the first on September 29–30 1983 and the second on January 27–28 1985. The total bandwidth was 100 MHz, split into two 50 MHz bands centered on 1465 and 1515 MHz. The source 3C 286 was used as a primary flux calibrator and other calibrator sources were observed for 5 minutes every half hour. Because our sources were selected from fields at 0^h (SA 68), 9^h (Lynx), 13^h (SA 57) and 17^h (Hercules), it was possible to observe in one continuous 24 hour block. Maps were made from a simple 5-minute observation for strong sources, and from up to three 10-minute observations for weak, extended ones.

The resulting maps typically had a noise of 0.15 mJy per half hour of observation and a resolution of 1$''$.4, although in some cases the maps were tapered in order to detect diffuse components. Due to the large bandwidth, the effective field of view of each map is only 25$''$, so the observations were restricted to only one source per map.

2.2. Data reduction

The initial calibration was carried out at the VLA site. Flux scales were calibrated using 3C 286, which has a total flux of 14.4 Jy at 1465 MHz (Baars et al.; 1977). Correcting for the fact that one extended component, containing a few percent of the total flux, is resolved out at 20 cm with the A-array, we used values of 13.8 Jy at 1465 and 13.5 Jy at 1515 MHz on the longer baselines. The final reduction was done using the Charlottesville (pre AIPS) VLA reduction package, adapted for use on the Amdahl V7B of the Leiden University computing center. Each 50 MHz channel was reduced separately and the CLEAN-ed maps were averaged.

In the reduction process, we profited greatly from the existing WSRT 21 cm maps of the LBDS fields. This enabled us to locate precisely all strong, nearby sources which cause confusion. If necessary, we made offset maps at the location of the interfering sources and decomposed them into CLEAN components. These were then subtracted from the map. For extended interfering sources this did not give very satisfactory results, because very large numbers of components would be required for a good representation.

Due to Earth-based interference and problems with the innermost telescopes (especially during the 1983 run), data from the shortest spacings sometimes had to be left out. If a source remained undetected or if it was suspected that not all the flux was recovered, a low resolution map was made by using a Gaussian tapering function, usually to 2$''$ or 3$''$.5 resolution.

The maps were cleaned to 1–3% of the peak. After cleaning, the components were restored with a circular beam. After averaging of the two channels, further analysis was done using the WSRT reduction package. Fluxes at 1412 MHz were calculated using 50-21 spectral indicates from Windhorst and Oppe (1986), or – if none was available – using a value of 0.75. Errors in position and flux were determined empirically by a direct comparison with the LBDS 21 cm and optical data (see appendix).

Source parameters were determined using a two dimensional elliptical Gaussian fitting routine for unresolved, resolved and slightly extended sources. For extended or complex sources a different procedure was used, described in Windhorst, et al. (1984) Sect. 4b II: The total flux of the source is determined directly from the data by summing the pixel intensities within the 1σ contour. If possible, the source is divided into components, for which the relevant parameters are calculated separately by hand. The angular size and position angle of the entire complex is determined from the relative positions of the outermost components.

No statistical corrections for noise induced overestimation of the source parameters were applied, because different conditions exist in each map. For the sake of uniformity, unresolved sources are therefore tabulated with a signal-to-noise independent upper limit of their angular size of 1$''$, except in cases where the resolution in the map was much lower. The *observed* (uncorrected) upper limits lie in the range of 0$''$.5 (for the highest signal-to-noise sources) to 1$''$. We have chosen the outer envelope of these upper limits to ensure that the angular sizes of the unresolved sources in our sample are all indeed smaller than the upper limit cited.

3. Description of the sample

3.1. Selection criteria and the source list

Our present sample is built up from two observation runs, $1\frac{1}{2}$ years apart. Although the two sets of observations were carried out with different direct goals in mind, they have two basic selection criteria in common, based on practical considerations. First of all, the total flux of each source must be greater than about 1 mJy in order to avoid prohibitively long observing times but

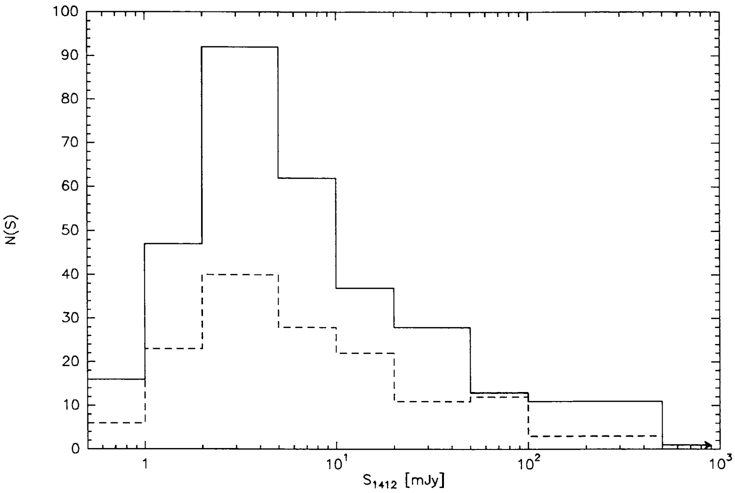

Fig. 1. The fluxdistribution of the VLA sample (dashed line) and that of the entire LBDS sample (solid line)

still allow mapping of marginally extended sources. For this reason, and because the field of view of the A-array when used at 20 cm for snapshots is limited to 30″, our second selection criterion was to map only sources with a largest angular size $\psi \leqq 20''$. Fortunately, the median angular size for sources with $S < 50$ mJy is equal to or less than 10″, so this does not introduce a very large bias. Moreover, sources larger than 20″ are resolved by the WSRT beam and we used the LBDS data of such sources to correct for this bias.

The observations of 8 of the 144 sources that were observed had so much interference either from a strong source nearby or from Earth-based signals that the data were useless. Three more sources were not detected. One of these is almost certainly a spurious LBDS detection (at only a 4σ level). The other two sources were too extended and/or diffuse. In contrast, two strong LBDS sources were detected in maps offset far from the field-center of observations of other sources. However, no accurate fluxes could be determined, because the attenuation of the primary beam is very uncertain at these distances. Thus, the final sample contains 133 LBDS sources, with a VLA peak flux $>3\sigma$, of which 85 are from the complete radio/optical LBDS sample, 11 were not in the radio complete sample and 37 were in the radio but not in the optical complete sample. Parameters for all these sources are given in Table 1a, b and c. Figure 1 shows the flux distributions of the present sample, as well as the total LBDS sample. Several LBDS sources turned out to consist of two or more components which, on the basis of several considerations, we consider to be separate sources. An explanation in each case is given in the notes following Table 1.

Table 1 is organized as follows:

Column 1: The source name in the LBDS complete sample. Sources which were defined as multi component sources in the LBDS sample are designated by an asterisk behind the source name. Each component is listed directly below. If one or more unrelated VLA sources were detected, the original LBDS name is given followed by a sequence number, e.g. xxWyyy.1.

Columns 2 and 3: The right ascension and declination of the source for equinox 1950. Errors are given directly below.

Columns 4 and 5: The total flux density at 1490 MHz and the flux transformed to 1412 MHz in mJy. Errors are given directly below.

Column 6: The largest angular size "ψ" (full width at half-maximum) in arcseconds.

Column 7: The position angle ϕ of the major axis ψ, measured in degrees from North to East.

Column 8: The optical identification. R = red, B = blue (for a definition, see sect. 5.1). G = Galaxy, Q = Quasar, ? = Uncertain identification.

Column 9: Notes. V: Source is probably variable; based on the following considerations: A) The source is known to be variable from WSRT observations at different epochs. B) The VLA total flux exceeds the WSRT flux by more than 3σ.
H: Source has a low surface brightness halo.
C: A contour plot is given in Fig. 13.
T: Source has a tail
+ or −: The difference between the LBDS and VLA total flux is greater than $2\frac{1}{2}\sigma$. A "+" is given if the WSRT flux is greater than the VLA flux.

3.2. Optical identifications

Because of the size of the WSRT beam($\sim 12\farcs5 \times 12\farcs5/\sin\delta$), it is unavoidable that deep optical identification programs will yield a few incorrect identifications. In the LBDS, where an identification was deemed correct when its likelihood ratio (i.e. the ratio between probabilities that an object is the correct identification or an unrelated background source) was greater than 2, the contamination fraction was estimated to be about 8% (Windhorst et al., 1984b). With our sample, where the uncertainty in the radio source positions is very much smaller than that of the optical positions, we can estimate the true contamination fraction in the LBDS. This is of vital importance, because an underestimation of this contamination can seriously affect the determination of the evolution of the ratio galaxy populations.

Of the 85 sources in the complete sample which we detected, 8 were identified incorrectly, giving indeed a contamination fraction of ~10%. However, when we examine the contamination of the different optical types separately, the differences are striking. 5 out of 30 of the blue galaxy identifications are incorrect on the basis of the VLA positions and an additional one was identified with the wrong component of a double galaxy (see notes), while only 3% (1 out of 34) of the red galaxies was incorrectly identified. One of the seven very faint identifications of

Table 1a. The VLA source list. Sources belonging to the radio/optically complete LBDS sample

WSRT name	RA (1950) HH dd mm.ss	DEC (1950) dd ' "	S(1490) [mJy]	S(1412) [mJy]	PSI "	PHI deg	ID	notes
54W014	0 13 40.14	15 34 40.4	4.45	4.63	1.1	34	?	- V
	0.01	0.1	0.22	0.23				
54W021	0 13 52.37	16 4 22.3	2.28	2.28	1.4	45	RG	
	0.01	0.1	0.30	0.32				
54W028	0 14 6.22	15 51 55.3	44.2	46.0	12.1	45	RG	C
	0.01	0.1	2.1	2.2				
54W038	0 14 28.48	15 53 59.1	5.53	5.76	3.5	28	RG	C
	0.01	0.1	0.68	0.74				
54W052	0 15 5.72	15 54 26.0	11.5	12.0	< 1.0		BG	
	0.01	0.1	0.5	0.5				
54W053	0 15 6.21	15 30 47.4	2.67	2.77	< 1.0		BG	
	0.01	0.1	0.15	0.16				
54W057	0 15 9.37	16 34 36.0	454.2	472.9	3.3	80	BG?	
	0.01	0.1	19.5	20.1				
54W065	0 15 31.81	16 19 13.0	1.83	1.90	< 1.0		BG	
	0.01	0.1	0.27	0.27				
54W067	0 15 34.91	16 20 56.7	54.1	56.4	7.6	5	BG	
	0.01	0.1	2.6	2.7				
54W079	0 15 56.32	16 4 4.9	228.5	237.9	5.1	60	?	
	0.01	0.1	9.5	10.2				
54W081	0 16 1.85	15 41 50.9	15.7	16.3	< 1.0		BG	
	0.01	0.1	0.7	0.7				
54W084.1	0 16 6.23	15 45 29.7	5.26	5.43	6.0	92	RG	
	0.02	0.2	0.91	0.93				
.2	0 16 6.92	15 45 26.2	7.47	7.78	3.5	0		
	0.04	0.4	1.25	1.27				
.3	0 16 6.86	15 45 16.8	3.43	3.57	3.8	67		
	0.07	0.7	1.14	1.16				
54W088	0 16 34.95	15 35 40.1	7.77	8.09	5.4	118	RG	
	0.02	0.2	1.32	1.37				
55W007	8 32 5.91	45 5 46.4	7.82	8.36	5.8	174	RG	C
	0.02	0.2	1.12	1.14				
55W016	8 33 20.09	45 16 48.5	4.29	4.59	5.9	129	RG	C
	0.01	0.1	0.64	0.65				
55W018.1	8 33 31.77	44 42 50.5	29.0	30.0	4.5	45	BQ	C
	0.01	0.1	1.4	1.4				
.2	8 33 31.73	44 42 46.0	2.15	2.20	1.1	150		
	0.01	0.2	0.18	0.18				
55W036	8 34 15.58	45 15 46.2	6.20	6.41	1.7	56	BG	
	0.01	0.1	0.59	0.60				
55W043.1*	8 35 14.24	44 57 38.8	4.96	5.21	7.2	102	RG	T
	0.03	0.3	1.00	1.02				
.1A	8 35 14.24	44 57 38.8	2.82	2.96	1.1	100		
	0.01	0.1	0.24	0.25				
.1B	8 35 14.87	44 57 37.3	2.14	2.25	4.3	117		
	0.02	0.2	0.46	0.48				
.2	8 35 14.53	44 57 45.6	2.78	2.92	4.0	146		
	0.02	0.3	0.99	1.04				
55W046	8 35 24.09	45 32 7.8	7.42	7.79	2.1	147	RG	
	0.01	0.1	0.46	0.47				
55W049	8 35 35.86	44 50 52.1	4.93	4.86	< 1.0		BG	
	0.01	0.1	0.24	0.24				
55W063	8 36 36.77	44 55 30.2	90.5	92.7	28.6	125	RG	+ C
	0.01	0.1	4.0	4.0				
55W066	8 36 52.35	45 16 19.9	20.0	20.8	8.1	38	BG	C
	0.04	0.4	1.8	1.8				
55W067	8 36 52.86	45 10 28.9	6.08	6.20	2.1	56	RG	-
	0.01	0.1	0.40	0.41				
55W068	8 37 3.84	45 15 25.1	3.84	4.13	1.1	90	RG	
	0.01	0.1	0.21	0.23				
55W077	8 37 30.48	44 45 18.7	8.75	9.03	< 1.0		BG	
	0.01	0.1	0.46	0.47				
55W092	8 38 13.42	45 6 54.0	3.10	3.32	7.3	98	RG	
	0.04	0.4	0.72	0.73				
55W093	8 38 17.71	44 48 51.9	1.10	1.14	1.2	45	RG?	
	0.01	0.1	0.27	0.28				
55W102	8 38 46.85	45 4 54.3	6.18	6.55	4.4	1	BG?	- H
	0.01	0.1	0.52	0.54				
55W105	8 38 48.57	45 21 31.8	3.47	3.57	< 1.0		RG	
	0.01	0.1	0.22	0.24				
55W111	8 39 28.42	45 14 11.8	6.72	6.49	< 1.0		?	
	0.01	0.1	0.28	0.29				
55W124	8 40 50.98	44 49 45.1	3.66	3.75	< 1.0		BQ	- V
	0.01	0.1	0.18	0.19				
55W125.1	8 40 52.11	44 22 9.0	14.9	15.1	< 1.0		BQ?	
	0.01	0.1	0.7	0.7				
.2	8 40 52.45	44 22 19.1	2.58	3.44	2.4	86		
	0.01	0.1	0.38	0.40				
55W135	8 41 17.64	44 32 30.7	1.35	1.40	1.8	106	SP	-
	0.01	0.1	0.30	0.31				
55W144	8 41 54.06	45 12 11.3	1.89	1.95	3.5	113	BG	
	0.03	0.3	0.36	0.36				
55W149	8 42 2.92	45 6 22.9	6.51	6.81	10.1	156	RG	C
	0.04	0.4	0.98	1.00				
55W154	8 42 17.49	44 51 9.4	8.94	9.21	14.6	81	RG	C
	0.03	0.3	1.12	1.15				
55W166	8 43 12.70	44 41 54.1	2.47	2.60	< 1.0		RG	
	0.01	0.1	0.15	0.16				
55W165*	8 43 12.90	44 52 44.8	14.2	15.7	34.2	82	Q?	C
	0.11	1.1	3.2	3.3				
A	8 43 11.23	44 52 42.5	6.12	6.26	5.4	32		
	0.07	0.7	1.5	1.5				
B	8 43 13.91	44 52 46.8	8.06	9.48	4.0	112		
	0.05	0.4	1.51	1.70				

Table 1a (continued)

WSRT name	RA (1950) HH dd mm.sss	DEC (1950) dd ' "	S{1490} [mJy]	S{1412} [mJy]	PSI "	PHI deg	ID	notes
55W171	8 43 43.32	44 33 46.7	3.50	3.48	< 1.0		BG	V
	0.01	0.1	0.17	0.17				
55W175	8 44 10.61	44 15 13.4	41.5	40.4	< 1.0		BG	
	0.01	0.1	1.8	1.7				
55W184	8 44 39.63	44 39 31.3	0.50	0.51	< 1.0		BG?	
	0.01	0.1	0.10	0.10				
55W188	8 45 3.01	44 51 35.2	7.68	7.98	4.0	45	BG	-
	0.01	0.1	0.35	0.39				
55W190	8 45 14.16	44 40 47.1	13.5	13.9	1.8	130	RG?	+
	0.01	0.1	0.8	0.8				
55W191	8 45 16.57	44 13 3.3	13.6	14.1	< 1.0		BG	
	0.01	0.1	0.6	0.6				
55W199	8 45 42.76	44 32 30.0	2.24	2.34	4.2	70	BG?	
	0.04	0.4	0.52	0.53				
55W200	8 45 43.78	44 13 35.1	2.84	2.89	2.0	92	RG	- H
	0.01	0.1	0.27	0.28				
55W210	8 46 12.54	44 32 41.4	1.54	1.58	2.1	95	RG	
	0.02	0.2	0.30	0.31				
55W226	8 47 35.75	44 34 39.7	4.15	4.28	< 1.0		BG	- V
	0.01	0.1	0.22	0.23				
52W005	13 4 27.46	29 31 18.7	13.0	13.4	7.0	85	BG	+ C
	0.09	0.9	1.7	1.8				
52W008	13 5 0.71	29 18 27.0	17.0	16.8	< 1.0		BG?	
	0.01	0.1	0.8	0.8				
52W012	13 5 23.82	29 19 3.1	6.31	6.71	3.6	28	BG	-
	0.01	0.1	0.62	0.64				
52W013	13 5 26.33	29 41 48.1	2.76	2.84	< 1.0		RG	
	0.01	0.1	0.14	0.15				
52W020	13 5 57.56	30 0 2.8	2.83	3.00	< 1.0		BG	
	0.01	0.1	0.14	0.16				
52W022	13 6 10.71	29 50 21.8	4.82	4.95	< 1.0		B?	
	0.01	0.1	0.23	0.24				
52W023	13 6 11.63	29 42 32.9	0.75	0.81	4.5	119	BG	
	0.03	0.3	0.24	0.24				
52W037	13 6 53.25	29 38 3.1	2.87	3.03	9.2	151	SP	
	0.12	1.2	0.25	0.26				
52W038	13 6 55.80	29 22 46.0	2.71	2.76	4.2	113	RG	-
	0.01	0.1	0.39	0.39				
52W039	13 7 1.30	30 2 3.5	3.00	3.18	5.3	178	R?	
	0.01	0.1	0.25	0.26				
52W047	13 7 43.24	29 42 15.4	50.5	51.5	< 1.0		BQ	+
	0.01	0.1	2.1	2.2				
53W005.1	17 13 22.25	50 31 43.2	6.22	6.60	11.9	109	BG	
	0.05	0.6	1.05	1.10				
.2	17 13 22.69	50 31 52.3	1.90	2.02	2.4	50		
	0.01	0.1	0.40	0.42				
53W008	17 13 47.95	49 57 36.4	285.3	297.7	1.9	102	BQ	
	0.01	0.1	12.0	12.4				
53W014	17 14 2.38	50 3 48.0	7.18	6.87	2.9	70	B?	
	0.01	0.1	0.85	0.84				
53W020	17 14 34.25	50 28 15.1	2.29	2.42	4.0	26	RG	-
	0.01	0.1	0.29	0.30				
53W024	17 14 55.47	50 0 0.2	5.32	5.48	< 1.0		BQ	- V
	0.01	0.1	0.33	0.34				
53W026	17 15 12.23	49 50 24.6	16.2	16.8	3.5	58	BG	C
	0.03	0.3	2.0	2.0				
53W029	17 15 14.65	50 23 33.8	20.6	20.3	< 1.0		BQ	
	0.01	0.1	0.9	0.9				
53W031	17 15 30.63	49 59 54.9	97.7	101.4	4.1	143	RG	
	0.01	0.1	4.0	4.4				
53W035	17 15 41.09	50 21 49.3	3.25	3.17	< 1.0		B?	- V
	0.01	0.1	0.23	0.22				
53W039	17 15 47.66	50 28 38.3	1.29	1.35	4.4	133	RG	- H
	0.05	0.5	0.41	0.42				
53W046	17 16 38.16	50 10 57.1	61.1	63.4	3.2	157	RG	C V
	0.01	0.1	2.6	2.8				
53W047	17 16 53.49	50 25 49.2	23.3	24.0	1.5	90	RG	
	0.01	0.1	0.9	1.0				
53W048	17 16 56.84	50 27 5.5	9.96	10.4	3.7	83	RG	
	0.01	0.1	0.85	0.9				
53W052	17 17 18.70	50 1 55.8	8.93	9.30	1.4	100	RG	
	0.01	0.1	0.44	0.46				
53W062	17 18 16.56	50 2 5.1	1.12	1.14	< 1.0		BG	V
	0.01	0.1	0.12	0.12				
53W065	17 18 24.64	50 0 37.4	4.85	5.18	< 1.0		BG	
	0.01	0.1	0.25	0.26				
53W071	17 18 56.81	50 20 12.9	4.44	4.80	< 1.0		BG	+ V?
	0.01	0.1	0.23	0.24				
53W072	17 19 15.30	50 25 32.1	5.17	5.22	< 1.0		SP	
	0.01	0.1	0.23	0.24				
53W075	17 19 26.36	49 46 42.6	92.4	96.3	< 1.0		BQ	
	0.01	0.1	4.0	4.1				
53W076	17 19 39.79	49 42 55.8	1.76	1.84	2.1	61	RG	
	0.01	0.1	0.36	0.36				
53W078	17 20 3.10	50 6 26.2	0.60	0.63	4.3	150	RG	- V
	0.01	0.1	0.14	0.14				

Table 1a (continued)

WSRT name	RA (1950) HH dd mm.sss	DEC (1950) dd ' "	S(1490) [mJy]	S(1412) [mJy]	PSI "	PHI deg	ID	notes
53W079	17 20 8.02	50 13 22.0	12.1	12.2	< 1.0		RG	
	0.01	0.1	0.5	0.5				
53W080	17 20 22.14	49 58 26.8	18.6	19.5	10.4	9	BQ	- C
	0.01	0.1	1.1	1.2				
53W083	17 20 33.89	50 5 28.9	5.23	5.43	< 1.0		BG	
	0.01	0.1	0.29	0.29				
53W085	17 20 37.05	49 57 23.1	3.82	4.09	< 1.0		BQ	
	0.01	0.1	0.19	0.21				
53W086.1	17 20 42.22	49 56 22.7	3.11	3.17	2.5	144	RG	
	0.01	0.1	0.35	0.36				
2	17 20 40.94	49 56 28.5	1.73	1.77	2.8	102		
	0.01	0.1	0.29	0.29				

Notes on individual sources in Table 1a

54W053: The optical and VLA radio positions differ by 8.″5. It is probably an incorrect identification
54W065: The optical and VLA radio positions differ by 3.″5. It is probably an incorrect identification
54W084: The LBDS radio sources consists of three VLA sources: Two doubles and one head-tail source. The optical identification coincides with component No. 1
55W018: This complex consists of a strong double (component 1) with the optical id at the position of the strongest peak. Component 2 is a small, much weaker, elongated feature extending from component 1. It may be a background source
55W043: This source consist of three parts. Component 1A is a marginally resolved, strong source which coincides with the optical position. Component 1B is a weaker extended component, elongated towards component 1A. They are probably parts of one radio source. Component 2 lies 8″ to the North of 1A, almost perpendicular to the direction connecting components 1A and B. It is probably an unrelated source
55W063: This source has a large, diffuse tail trailing a strong resolved peak. The angular size and flux are much larger than was found in the LBDS. There is a small possibility that the tail is caused by interference in the VLA map
55W093: The optical position lies 5″ away from the marginally resolved source. No flux difference is seen between the LBDS and VLA, so an undetected, diffuse component at the optical position is unlikely. Probably an incorrect identification
55W111: The LBDS source has an angular size of 14″, while the VLA source is unresolved. There is, however, no flux discrepancy. Possibly error in the LBDS angular size
55W125: This source has two components, probably unrelated. Component 1 is a strong, unresolved source coinciding exactly with the optical identification. Component 2 lies 12″ away and is elongated in a direction perpendicular to the direction toward component 1
55W135: Only very diffuse, low flux density emission is detected. A large amount of flux is missing and is probably diffuse as well
55W165: This is an extremely complex source with three possible optical identifications. There are no definite indications that it is one source, but only the identification of the western component seems correct
55W184: The optical position of this source lies 4″ away from the VLA source. However, half of the LBDS flux is missing, and it is possible that there is diffuse emission present at the optical position. It was not detected, though, not even in the low resolution map
55W191: The optical and VLA radio positions differ by 3″ (6σ position offset). Probably an incorrect identification
52W008: This source has a LBDS angular size of 17″. The only detected VLA source is unresolved, but 20% of the LBDS flux is missing
52W023: The optical and VLA radio position differ by 7″. Probably an incorrect identification
52W038: This source has a LBDS angular size of 12″ and has a tail which should have been seen in the VLA map. Only an unresolved source, coinciding with the optical position was detected, however. The shape of the LBDS source is strange, and the tail may not be real
53W005: This source consists of 2 components. Two subcomponents make up source 53W005.1. The optical id lies midway between the two subcomponents. The second component lies 12″ away from the first complex. The optical id of component 1 lies in a group of galaxies, so it is possible that the optical id of component 2 lies in the same group
53W035: The LBDS source is resolved (7″), but the VLA maps show only an unresolved component. There is a flux discrepancy of 20%, however, so there is probably a diffuse component
53W065: The optical and VLA radio positions differ by 3″. Probably an incorrect identification
53W086: This source consists of two components, 13″ apart. The optical position coincides with component 1. The two components are probably unrelated

Table 1b. Sources from the complete radio LBDS sample, unidentified on 4m plates

WSRT name	RA (1950) HH dd mm.ss	DEC (1950) dd ' "	S(1490) [mJy]	S(1412) [mJy]	PSI "	PHI deg	ID	notes
54W011	0 13 23.85	15 34 39.3	5.14	5.35	< 1.0			
	0.01	0.1	0.20	0.25				
54W023	0 13 58.37	15 31 3.2	9.74	10.2	6.2	133		
	0.01	0.1	0.33	0.5				
54W024	0 14 0.31	15 30 35.5	1.64	1.71	2.0	177		
	0.01	0.1	0.30	0.30				
54W033	0 14 19.75	15 30 30.2	9.42	9.81	2.6	49		
	0.01	0.1	0.45	0.48				
54W046	0 14 44.72	15 42 30.2	14.7	15.4	2.7	132		
	0.01	0.1	0.8	0.8				
54W051	0 15 2.79	15 41 40.2	3.23	3.36	1.1	144		
	0.01	0.1	0.18	0.19				
54W059	0 15 16.61	15 39 26.9	1.57	1.62	< 1.0			
	0.01	0.1	0.11	0.12				
54W060A	0 15 20.48	15 45 5.3	1.24	1.29	< 1.0			
	0.01	0.1	0.13	0.13				
54W060B	0 15 22.26	15 44 51.3	4.22	4.22	2.5	129		
	0.07	0.7	1.12	1.13				
54W061	0 15 24.59	15 25 18.4	26.1	27.1	5.7	82		+ C
	0.01	0.1	1.1	1.3				
54W066.1	0 15 33.67	15 47 0.8	1.22	1.27	2.1	120		
	0.02	0.2	0.31	0.32				
.2	0 15 33.71	15 46 48.7	1.01	1.05	< 1.0			
	0.01	0.1	0.15	0.16				
54W075	0 15 52.00	15 49 11.8	3.69	3.85	1.7	45		
	0.01	0.1	0.30	0.31				
55W133	8 41 13.71	44 36 54.6	1.69	1.84	< 1.0			
	0.01	0.1	0.14	0.15				
55W201	8 45 44.69	44 31 33.1	1.64	1.75	3.2			
	0.03	0.3	0.52	0.53				
55W203	8 45 47.92	45 1 17.3	178.2	187.2	< 1.0			
	0.01	0.1	8.0	8.0				
53W002	17 12 59.76	50 18 51.6	46.6	49.4	< 1.0			
	0.01	0.1	1.9	2.1				
53W004	17 13 21.46	50 13 46.1	53.0	53.5	< 1.0			
	0.01	0.1	2.3	2.4				
53W012	17 13 53.51	50 3 43.5	55.0	56.2	20.6	175		C
	0.01	0.1	4.6	4.7				
53W037	17 15 45.09	50 22 25.7	4.67	4.68	9.6	109		- H
	0.02	0.2	0.55	0.56				
53W041	17 16 3.19	49 52 26.5	2.10	2.18	< 1.0			- V?
	0.01	0.1	0.26	0.27				
53W042	17 16 8.08	49 51 33.9	4.76	5.05	3.3	68		
	0.02	0.2	0.83	0.85				
53W043	17 16 15.09	50 22 0.2	3.12	3.38	2.5	176		
	0.01	0.1	0.23	0.24				
53W049	17 16 57.36	50 36 18.2	97.6	101.9	27.8	65		C
	0.01	0.1	4.5	4.6				
53W055*	17 17 34.01	50 42 54.2	14.7	15.6	16.4	134		
	0.01	0.2	2.6	2.8				
A	17 17 34.51	50 42 48.7	5.73	6.08	4.2	120		
	0.01	0.1	1.00	1.03				
B	17 17 33.58	50 42 58.9	8.92	9.47	7.3	128		
	0.01	0.1	1.65	1.70				
53W057	17 17 51.28	49 48 45.5	1.96	1.93	1.1	90		
	0.01	0.1	0.18	0.18				
53W059	17 18 5.10	50 3 18.7	15.5	16.2	< 5.0			V
	0.01	0.1	0.9	1.0				
53W060	17 18 8.27	49 31 43.8	8.26	8.81	< 1.0			
	0.01	0.1	0.37	0.39				
53W066	17 18 27.66	50 4 2.3	3.85	4.04	< 1.0			
	0.01	0.1	0.20	0.20				
53W067	17 18 36.79	50 13 52.6	21.2	22.1	12.5	120		C
	0.01	0.1	0.9	1.0				
53W069	17 18 46.45	49 47 47.6	1.55	1.62	3.8	30		- H
	0.01	0.1	0.28	0.29				
53W070	17 18 51.12	50 8 57.9	2.50	2.49	< 1.0			
	0.01	0.1	0.15	0.15				
53W081	17 20 22.56	50 0 47.6	11.8	12.5	< 1.0			
	0.01	0.1	0.6	0.6				
53W082	17 20 22.85	50 11 17.3	2.89	3.12	< 1.0			+ V?
	0.01	0.1	0.17	0.18				
53W087	17 20 44.29	50 11 31.8	3.93	4.13	1.7	100		- H?
	0.01	0.1	0.51	0.52				
53W088	17 20 44.22	50 14 41.6	11.2	11.1	< 1.0			- V?
	0.01	0.1	0.5	0.5				
53W089	17 20 46.26	50 9 41.4	1.99	2.13	3.0	175		
	0.04	0.4	0.63	0.64				
53W091	17 21 17.81	50 8 47.4	26.9	29.5	4.2	131		+
	0.01	0.1	1.4	1.4				

Notes on individual sources in Table 1b

54W060A/B: The two components of the LBDS complex 54W060 were observed separately. They are two unrelated sources

54W066: This complex consists of two unrelated sources, 15″ apart. The separation could not be made in the LBDS source, because the two components lie exactly North-South, a direction in which the WSRT beam is very elongated at this declination

Table 1c. Miscellaneous other sources from the LBDS

WSRT name	RA (1950) HH dd mm.ss	DEC (1950) dd ' "	S(1490) [mJy]	S(1412) [mJy]	PSI "	PHI deg	ID	notes
54W005*	0 12 52.73	16 33 28.6	20.4	21.0	15.3	81	RG?	C
	0.01	0.1	3.6	3.7				
A	0 12 52.73	16 33 28.6	6.51	6.71	4.2	111		
	0.01	0.1	1.45	1.46				
B	0 12 51.85	16 33 26.5	13.9	14.3	7.6	73		
	0.01	0.1	3.0	3.1				
54W056	0 15 8.74	15 37 25.4	1.22	1.27	< 1.0		BG	
	0.01	0.1	0.13	0.13				
54W068A.1	0 15 34.47	16 32 39.6	9.78	10.2	<1.0		BG?	
	0.01	0.1	0.45	0.5				
.2	0 15 34.12	16 32 40.3	3.64	3.79	<1.0			
	0.01	0.1	0.42	0.44				
55W109	8 39 19.91	45 16 23.4	10.3	10.7	14.8	117	RG	
	0.02	0.3	1.0	1.1				
55W114	8 40 8.99	44 57 28.0	0.88	0.94	< 1.0		BG?	
	0.01	0.1	0.10	0.11				
55W161B	8 43 4.00	44 40 57.0	1.77	1.93	2.1	103	RG	
	0.01	0.1	0.11	0.13				
55W168	8 43 33.63	44 29 49.9	1.90	2.04	< 1.0		BG?	
	0.01	0.1	0.14	0.14				
52W019	13 5 57.34	29 22 19.2	1.63	1.71	< 1.0		BG	
	0.01	0.1	0.19	0.20				
52W024	13 6 14.99	30 7 6.9	10.1	10.4	4.5	68	RG	C
	0.02	0.2	1.9	1.9				
52W036*	13 6 50.23	29 40 25.0	1.24	1.32	3.7	148	BG?	
	.02	0.2	0.41	0.42				
A	13 6 50.13	29 40 26.8	0.77	0.81	2.2	180		
	0.02	0.2	0.29	0.30				
B	13 6 50.32	29 40 23.1	0.48	0.50	1.8	135		
	0.02	0.2	0.17	0.17				
53W019	17 14 32.66	50 33 21.7	10.7	11.1	25.2	175	RQ?	
	0.12	1.3	1.6	1.7				
55W103	8 38 47.66	45 23 14.2	-----	----	10.9	30		
	0.01	0.1						
55W211A	8 46 16.06	44 34 24.6	-----	----	6.0	57		
	0.01	0.1						

Notes on individual sources in Table 1c

55W109: The optical identification of this source was not included in the optical complete sample because of its low likelihood ratio. It does, however, coincide exactly with the strong peak in the VLA map.

55W103/55W211A: These sources were detected in maps centered on other sources. Due to the large attenuation, no accurate fluxes could be determined

uncertain type was incorrect and all the spirals (4) and quasars (11) were identified correctly. Two sources which were rejected from the complete optical sample are definitely correct identifications: one red galaxy and one quasar. The marked difference in contamination fraction must be due to the fact that Windhorst et al. (1984b) used a background density of objects on the 4m plates which is independent of type.

We must conclude, therefore, that using a type independent likelihood ratio introduces a bias in an optical complete sample. This bias is significant when using positions from relatively low resolution (e.g. WSRT) maps and when searching to very faint magnitudes. High resolution observations of the type presented here eliminate this bias.

3.3. *Variable and diffuse sources*

Before we start with the morphological analysis of the sample, a few words must be said about the large flux differences between some of the LBDS sources and the fluxes found from the VLA maps. A large fraction of these sources are variable, and in majority unresolved quasar cores. They are denoted by a "V" in the notes of Table 1. For extended sources, the difference is generally caused by the fact that with the ten-fold increase in resolution of the VLA maps, low level diffuse flux may have been missed. In the further analysis we will use the WSRT total fluxes in these cases. Only a few sources remain where neither of the simple reasons above apply. These sources are commented on in separate notes. They are mostly sources which are much smaller in the VLA maps than is indicated by the WSRT map, but where the extra component should have been detected. Because it concerns only a small minority in the sample and because tapered maps did not show an increase in flux either, we used the parameters from the VLA maps.

4. Median angular sizes

One of the interesting occurrences at low flux densities is that the median angular size of radio sources, after staying almost constant at $\sim 10''$ from about 1 Jy downwards, seems to drop off sharply to $\sim 3''$ at a few mJy (Oort and Windhorst; 1985). Because this decrease occurs at the same flux densities where the so-called "upturn" in the source counts at 1.4 GHz is seen, it is important to know if these two features are caused by the same effect, i.e. the emergence of the blue population of radio galaxies.

We can answer this question by taking our sample and using the LBDS complete sample as a basis for correcting for the slightly different distribution of optical classes of the VLA sample, and for its cutoff in angular size. First of all, we correct for the lack of large sources by adding the LBDS sources with $\psi > 20''$ to our sample. Because we have observed only part of the LBDS sources with $\psi < 20''$, each LBDS ($\psi > 20''$) source was given a weight which is equal to the ratio of the total number of LBDS ($\psi < 20''$) sources and the number observed with the VLA. Two

Table 2. Observation statistics of the different optical types. *Column 1:* Number of $\psi \leqq 20''$ sources observed with the VLA. *Column 2:* Total number of $\psi \leqq 20''$ sources in the LBDS. *Column 3:* Number of sources with $\psi > 20''$ in the high declination LBDS fields. *Column 4:* Total number of $\psi > 20''$ sources in the LBDS

	$\psi < 20''$		$\psi > 20''$	
Type	No in VLA sample	No in LBDS sample	No in LBDS at high δ	No in total LBDS sample
Blue galaxies	30	36	3	7
Red galaxies	34	49	5	11
Quasars	11	25	8	8
Unidentified	35	111	1	5
Other	10	21	7	17

sources were observed with the VLA which had $\psi_{\rm LBDS} > 20''$. The VLA parameters were substituted for the WSRT values in these cases. Furthermore, the following proviso is made. Because extended sources of the low declination fields SA 68 and SA 57 have poorly determined angular sizes due to the large ellipticity of the WSRT beam at these declinations, and because they frequently turn out to be composed of two unrelated sources, we will use extended sources from the high declination part of the LBDS only ($\delta > 40°$).

Next, we correct for the fact that our sample is not a pro rata subset of the different optical types in the LBDS by again simply assigning a weight to each source which is proportional to the ratio of the number of sources of the same optical type in our sample and the number in the LBDS with $\psi < 20''$ of this type. Table 2 gives the number in the VLA and LBDS sample of each optical type. Sources in the VLA sample which are not part of the LBDS complete sample have not been included.

Before we proceed, a few words of caution are in order on the determination of the largest angular size. For multi-component sources the definition is clear and the calculation of ψ is straightforward. At high resolution, sources consisting of only one component are especially at low flux densities frequently diffuse, and certainly not Gaussian in shape. A precise determination of ψ is extremely difficult in these cases. We have used the traditional definition of the full width at half maximum along the major axis. This discriminates against sources with a large, low surface brightness halo. Therefore, we will underestimate ψ in some cases. This is most severe for sources with a total flux less than 5 mJy which have angular sizes $> 3''$. The discrepancy between the WSRT and VLA flux can amount to as much as 20%. For the large majority of the sources, however, the difference is less than 10%, even for the weaker sources. The effects on the median angular size will therefore be small.

Figure 2 shows the angular size vs. flux for the entire sample. In determining the median angular size, however, we will separate the sample into two flux ranges, sources with $S > 10$ mJy, and sources with $S \leq 10$ mJy. We have chosen this separation, because at 10 mJy the blue radio galaxies begin to dominate the source counts. We will calculate the integral $h(\psi)$ and differential $g(\psi)$ size distributions for those two categories separately, using the appropriate weights for each.

Let us first consider a subsample of sources with $S > 10$ mJy, which contains 58 sources which have either been mapped with

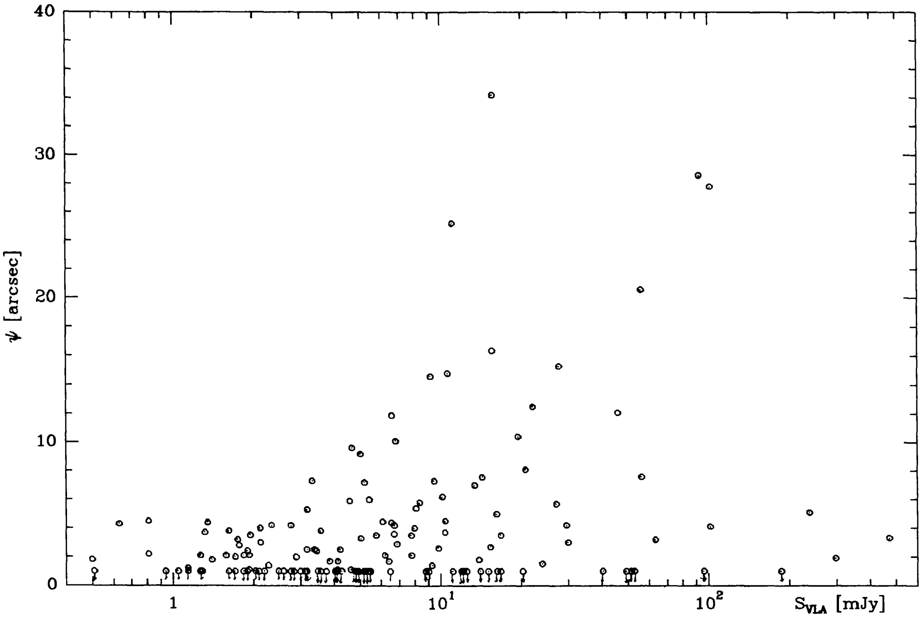

Fig. 2. The distribution of largest angular size as a function of flux density of the entire VLA sample. Note that the sample is incomplete for $\psi > 20''$

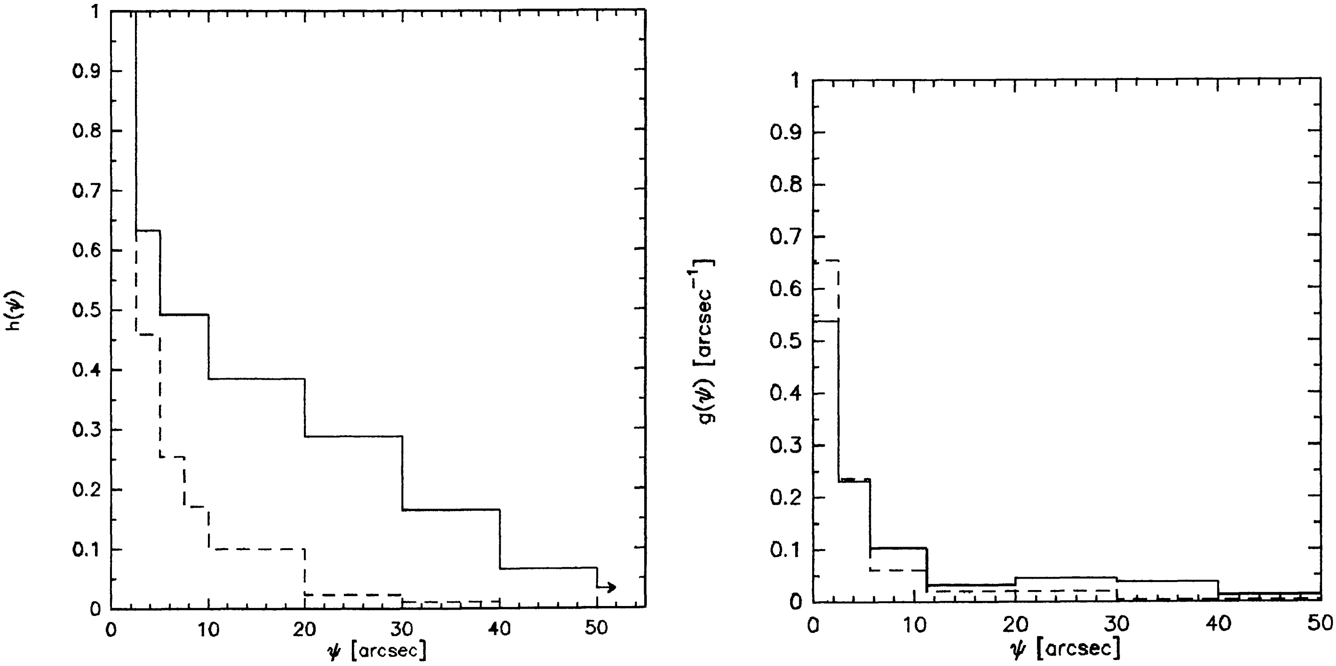

Fig. 3. **a** The integral size distribution $h(\psi)$ for $S^{1412} \geq 10$ mJy (solid line) and for $S^{1412} < 10$ mJy (dashed line). **b** The differential size distribution $g(\psi)$ for the same flux ranges. Only the sources which belong to the LBDS radio complete sample are used

the VLA or are extended, high declination LBDS sources. The integral and differential size distributions are plotted in Fig. 3(a) and (b). The median flux density of this subsample is 40 mJy. This is because very strong sources are few and far between and the LBDS fields cover only a very small area of the sky which is almost devoid of very bright sources. In this subsample, underestimation of ψ is not much of a problem because the signal to noise is sufficiently high to detect even components which are only 10% of the brightest peak. Moreover, if we were in doubt whether two components were related, we assumed them to be parts of a single source with the corresponding ψ. Even so, the median angular size we find ($\psi = 5'' \pm 1''$) is about a factor of 2 lower than the values found with lower resolution surveys, which is about 10″ over a large range in flux. Although a small part of this difference might still be caused by a remnant of a resolution bias in our sample, one main reason of this difference is the fact that frequently very extended sources turn out to consist of a number of small sources, which seem not to be related to each other because of their large separation in the VLA map, the absence of diffuse flux connecting the components, and because the position of the optical identification makes a connection between the components improbable. Some examples are shown in Fig. 13. Another reason for the difference in median angular size determined from low resolution observations and our determination may be that the median angular size whatever its precise value – is much smaller than the beam of the low resolution observations. It seems that in that case the value of $\psi_{\rm med}$ is overestimated, because sizes smaller than $\sim\frac{1}{2}$ HPBW cannot be determined accurately.

These deviations are amplified when we consider the low flux subsample. At $S < 10$ mJy, the median angular size drops to only 2″ (at a median flux of ~3 mJy), lower than was found using the VLA deep survey of the LBDS field Lynx.2 (Windhorst et al. 1985) who found a value of 7″.5 at 15″ resolution, and is consistent with what was found by Oort and Windhorst (1985), who found an upper limit of 5″ at 12″ resolution (at 2 mJy). It is also somewhat smaller than the median of ~6″ found by Coleman and Condon (1985) with a 6″ beam. It must be noted, however, that our value may be a slight underestimation, due to the fact that in this flux density range our angular size determination is affected by the non-detection of low surface brightness components in some cases. But, even if we take the LBDS angular sizes for the sources with a large amount of missing flux, the median angular size is still no more than 3″. This is because the sources where the difference between the LBDS and VLA flux is largest, are the sources which have VLA angular sizes which are higher than the median. An underestimation of their angular size only results in a change in the distribution of the angular sizes of the radio sources above the median, but *not* in a change in the median itself.

This decrease in angular size is probably caused by the emergence of the blue population of radio galaxies. In the next section it will be shown that this is indeed the case. Part of the decrease is also due to a decrease in angular size of the red galaxies, which, because it is not accompanied by an average increase in redshift, are physically smaller than their high-flux counterparts.

5. Radio galaxy populations

We will now have a more detailed look at the radio galaxy populations. The classical population of elliptical "red" galaxies serves as a good basis for morphological studies because they are "standard candles" i.e. one can make a reliable estimate of the redshift from their optical magnitudes (see van der Laan et al., 1985). A second important constituent of the radio galaxy populations especially at low fluxes are the "blue" galaxies, of which we know relatively little. They are distinguished from the red galaxies via a $(J - F)$ color vs. F magnitude relation calibrated through bulge-to-disk ratios (Kron et al., 1985). The blue

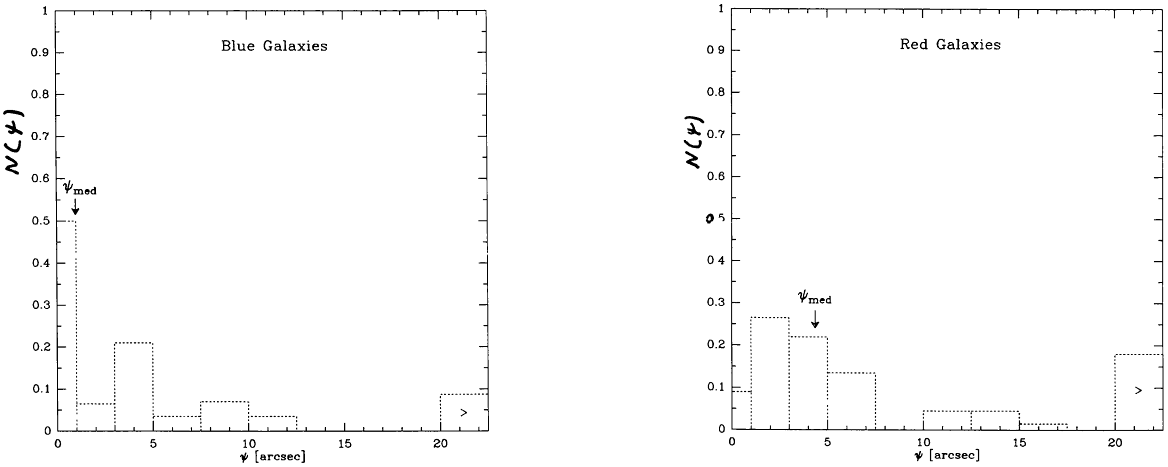

Fig. 4a and b. The angular size distribution of the blue (**a**) and red (**b**) radio galaxies, normalized to the total number of radio galaxies of each class in the LBDS. The "<" denote upper limits in the angular size. The arrows indicate the median in the distribution

galaxies were considered to be a new class of radio galaxy because locally ($z < 0.2$) they are 10–100 times as numerous as radio selected Seyferts and 10–30 times as powerful at radiofrequencies than spiral galaxies. Moreover, they often have peculiar optical morphologies. At higher redshifts, we know very little about the optical characteristics of the populations of radio galaxies. It is quite possible that the blue galaxy population consists of a number of different types of galaxy, having only their "non-red" colors in common. For instance, it has been suggested that high redshift Spirals and Seyferts account for the blue radio galaxies at flux densities below 1 mJy (Condon; 1984). The influence of the blue galaxies already starts at 50 mJy, however, and this cannot be explained with the known populations alone. Using our high resolution sample we can make a detailed study of the radio morphological differences between red and blue galaxies and maybe even distinguish the different sub-populations of blue galaxies.

5.1. *Red vs. blue galaxies*

The red-blue distinction in radio galaxies is made purely on optical grounds, using an empirically derived color-magnitude relation: A red galaxy is defined as having a $J(4600\,\text{Å}) - F(6200\,\text{Å})$ color larger than 1.2 for $F < 18$, and $J - F > 0.2F - 2.4$ for $F > 18$ (Kron et al., 1985). There were, however, indications that differences in the optical color are accompanied by differences in radio structure. A much larger fraction of the blue galaxies was unresolved by the WSRT beam (Kron et al., 1985).

One of the main reasons for our observations was to see if the radio structural differences were real. We can use the combination of our sample and the LBDS extended sources, using the same weights as in the previous section. The distribution of angular size $N(\psi)$ for blue and red galaxies is shown in Figs. 4(a) and (b). The distributions differ significantly. That of the red galaxies is broader, with almost no unresolved sources. The four unresolved red galaxies are redder than the boundary line defined above by less than 0.1 m (the uncertainty in $J - F$ is $\sim 0^{\rm m}.15$), so they may be blue galaxies, mis-classified due to either color errors, or to the uncertainty in the red/blue separating line (see Fig. 5). However, their optical luminosities are quite similar to those of ellipticals, and such a small color excess holds for a few very extended sources as well. The median angular size of the red radio galaxies in our sample is about $4''.5$.

The distribution of angular size of the blue galaxies, on the other hand, is much more strongly peaked toward low angular sizes, with 50% unresolved (i.e. $< 1''$). Note the three very extended LBDS blue galaxies, which are intriguing. Even if the angular sizes of these three sources are not overestimated by the low resolution observations, the median angular size is still $\leq 1''$ for all the blue galaxies. The uncertainties in the fluxes of the radio sources in our sample do not exclude the possibility that the unresolved sources have a diffuse component containing less than 10% of the total flux, which has not been detected in our maps. If this is the case, the full width at half maximum is not a good indicator of the size of a radio source. Even so, the morphology of the blue radio galaxies – with at least 90% of the flux in an unresolved nuclear component differs significantly from the morphology of the red radio galaxies.

Accepting the extended ($\psi > 1''$) blue galaxies to be really extended, it becomes interesting to investigate whether there are other properties which distinguish them from their unresolved blue counterparts. A straightforward analysis is complicated by three factors.

The main problem is that the redshift information for the blue radio galaxies is still very incomplete. What is more, the existing redshifts show that the absolute optical magnitudes cover a large range, making photometric redshift determinations (as used for the red radio galaxies) not very reliable. As a consequence, it is difficult to derive reliable intrinsic parameters. There are only six blue galaxies with a measured redshift; their large range of absolute magnitude prevents the determination of photometric redshifts.

Secondly, at very faint magnitudes, a quasar – galaxy distinction is difficult to make. It must be noted that blue galaxies with $(J - F) < 0.5$ (colors usually characteristic for quasars) occur only for $F > 21^{\rm m}.5$.

Despite these complications, there are indications that there are indeed intrinsic differences between the resolved and extended blue radio galaxies on the one hand, and the unresolved on the other. The ratio of resolved to unresolved blue galaxies decreases steadily with increasing flux, while the median F-magnitude stays roughly constant. This suggests a radiopower dependence on the

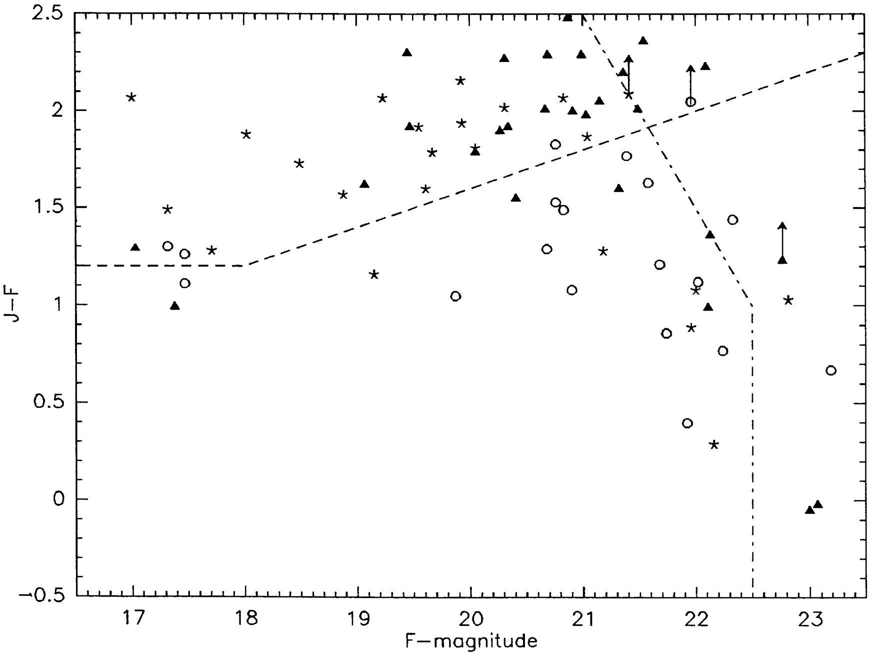

Fig. 5. The color-magnitude diagram for the radio galaxies from the current sample. Open circles are unresolved ($\psi < 1''$) sources, triangles are sources with $1'' \leqq \psi < 5''$ and asterisks are extended ($\psi \geqq 5''$) sources. The dashed line is the empirically determined boundary between red and blue radio galaxies. The dash-dotted line is the optical completeness limit

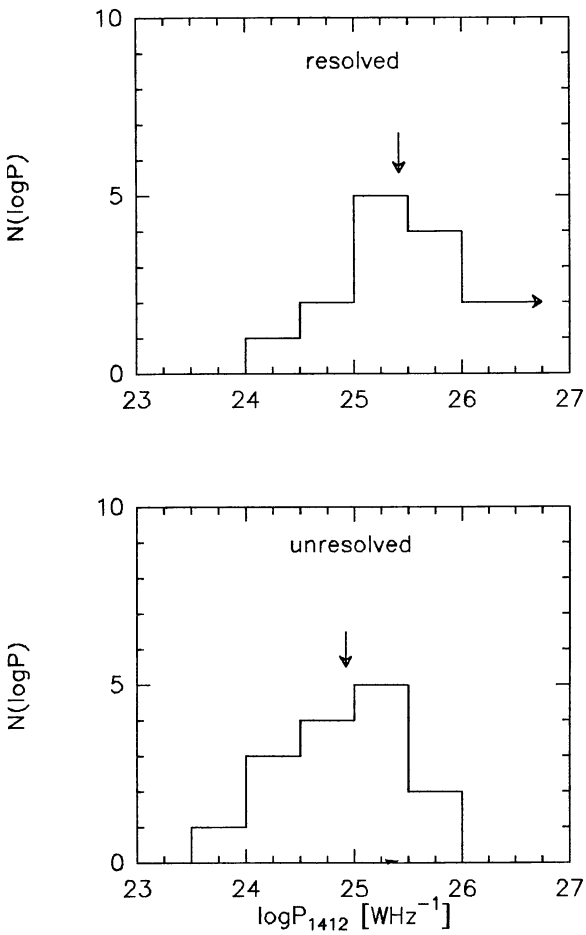

Fig. 6. The distribution in radio power of the resolved and extended (top) and unresolved (bottom) blue radio galaxies, for which redshifts were estimated, if not directly measured, by assuming $M_F = -22.5$. The arrows denote the median values

angular size of the radio source. We can try to test this by calculating a rough photometric redshift. From the blue radio galaxies with a measured spectroscopic redshift, we know their absolute magnitudes range from the giant elliptical luminosities to almost two magnitudes fainter, and have possibly a bimodal distribution. The median absolute magnitude of the distribution of absolute magnitude is $M_F = -22\overset{m}{.}5$, with a spread of $\sim 1\overset{m}{.}5$. We can assign the blue radio galaxies without a redshift an absolute magnitude of $M_F = -22\overset{m}{.}5$ and calculate photometric redshifts, taking the K-corrections into account. The resulting radiopower distributions show a median of 25.0 for the unresolved and 25.5 for the resolved and extended blue radio galaxies (Fig. 6). The sources with morphologies which resemble the classical elliptical double all lie at the high end of this distribution. It is quite possible that the sources which are more powerful in the radio are optically more luminous as well. In that case, we have *underestimated* their redshifts, which makes the difference in the radio power distributions even more marked.

Summarizing, there is a definite difference in angular size distribution between the red and blue galaxies which is not caused by distance effects. There is marginal evidence, which urgently needs further investigation, that there is an intrinsic difference between the blue galaxies unresolved in the radio and the resolved or extended ones.

5.2. *Blue galaxies vs. other populations*

As was shown in the previous section, we may assume that the population of blue radio galaxies is probably a mixed bag of several types of objects. We can attempt to compare the different characteristics with the known populations.

The radio-bright, extended blue galaxies seem to form a class by themselves. They are too luminous and radio-morphologically too unlike Spirals and Seyferts. On the other hand, they are too blue and optical-morphologically too distinct to be standard ellipticals. It is quite possible, though, that the high flux density

(> 10 my), extended blue radio galaxies, which (radio) morphologically resemble the red radio galaxies most, are associated with giant ellipticals with blue colors.

A large fraction of the blue radio galaxies show peculiar morphologies and are frequently interacting. It is possible that the radio emission we detect is a result of a recent encounter (see Kron et al., 1985).

Part of the unresolved blue radio galaxies could be explained by high redshift Seyfert galaxies, even though the Seyfert space densities seem much lower than those of the blue radio galaxies. Note that infrared selected Seyferts (de Grijp; private communication) seem to resemble closely both in radio morphology and radio power the unresolved blue galaxies. The number density of Seyferts is too small to account for the unresolved blue radio galaxies by a factor of 10–100 (Meurs, 1982), but IRAS selected Seyferts are at least three times more common than normal Seyferts and have the same radio luminosity range as the blue galaxies. Part of the unresolved blue galaxies may therefore be high redshift Seyferts. Still, Seyferts alone cannot explain the entire blue radio galaxy population. Moreover, recent spectral studies of blue galaxies (Windhorst et al., 1986) show no Seyfert-like spectra in a sample of 30 blue radio galaxies.

High redshift spirals are not likely to be a major contributor to the blue galaxy population at these flux levels. The radio luminosities of the blue radio galaxies for which we have measured spectroscopic redshifts are much higher than those of local spirals ($22 < \log P_{1.4} < 25$ for the blue radio galaxies vs. 20–22 for spirals). To explain the radio luminosity function of the blue radio galaxies at $z = 0.3$ entirely with high redshift spirals which are undergoing luminosity evolution, one requires evolution factors of $(1+z)^{10}$ or more. Such fierce evolution is seen only for the most powerful radio sources, and seems unlikely to occur in spirals. They may therefore contribute only to the low end of the blue radio galaxy radio luminosity function.

5.3. *Intrinsic properties of red radio galaxies*

In the absence of a sample with complete redshifts, the red galaxy population is the best homogeneous subsample of radio sources for studies of general intrinsic properties, because it is by now well established that one can estimate a photometric redshift fairly accurately ($\Delta z/z \approx 10\%$) at all flux densities (for references: see van der Laan et al., 1985) for redshifts up to 0.75. We can therefore in principle use these sources as a standard for a comparison with other populations. The subsample of red galaxies we will use in the following contains 43 sources of which 19 have a measured spectroscopic redshift. The others were assigned a photometric redshift based on an absolute F-magnitude which varies smoothly between -23.2 and -23.8 with $\Delta M \approx 0^m.6$. A Hubble constant of $50\,\mathrm{km\,s^{-1}\,Mpc^{-1}}$ and $q_0 = 0$ are assumed throughout.

We will investigate here the possible dependence of the linear sizes of radio sources associated with red radio galaxies vs redshift and radio power.

A small, but evident correlation between size and radio power was found by Gavazzi and Perola (1978) for two radio/optically complete samples of sources with redshift $z < 0.1$ from the 3C and B2 catalogues. Because this sample is at "local" redshifts, it can serve as a zero point for the study of a possible evolution of the median size of radio sources with redshift as well. Models for the space distribution as well as size distribution of the entire radio source population seem to require a general decrease of linear size with increasing redshift, if the observed flux density dependence of the median angular size is to be explained (Kapahi; 1975, 1986). However, so far *direct* evidence for such an effect has not yet been presented. Our sample, which contains sources in the redshift range $0.1 < z < 0.8$, may show – by comparison with the local sample of Gavazzi and Perola – whether size evolution indeed exists.

Because Gavazzi and Perola in general used a different definition for the largest angular size of a source (the size of the lowest contour in the radio maps), it was necessary to re-calculate the angular sizes in their sample according to our definitions. This has resulted in a small (~10%) decrease in the median angular size with respect to the values given in their paper.

Figure 7 shows the linear size vs. radio power of our subsample, together with the data of Gavazzi and Perola. Two differences between these two samples can be seen in this figure. First of all, the sizes in our sample are, on the whole, smaller than those of the local sample at the same radio power. As has been discussed in previous sections, this cannot be explained by a significant underestimation of the sizes in our sample, due to the presence of diffuse flux, which is resolved out in the VLA maps. Most of the sources in this subsample have high signal-to-noise ratios. The obvious explanation is, that there is indeed a decrease of the median linear size with redshift.

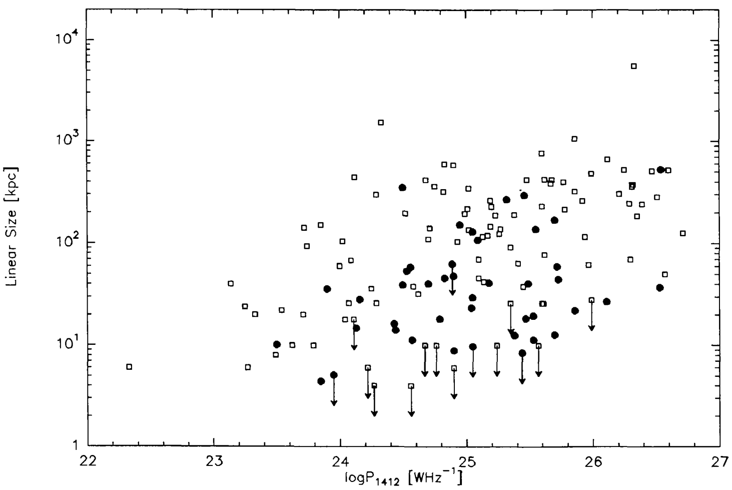

Fig. 7. Linear size (in kpc) vs radio power at 1.4 GHz (in W/Hz) for *red radio galaxies*. Open symbols are data from Gavazzi and Perola. Filled symbols are data from the present sample and the LBDS

Table 3. The value of the median linear size and redshift for intervals in radio power, for the three samples used in Sect. 5.3. *Column 1:* The radio power interval. *Column 2:* The median linear size in kpc. *Column 3:* The median redshift in the radio power interval. *Column 4:* Number of sources in the interval. *Column 5:* Number of sources with a measured spectroscopic redshift. *Column 6:* Sample used in the determination of the medians

$\log P$ (W/Hz)	$D^{\rm med}$ (kpc)	$z^{\rm med}$	N	$N^{\rm spec}$	Sample
23.5	30 ± 9	0.08	12	12	Gavazzi and Perola
24.5	75 ± 14	0.08	29	29	Gavazzi and Perola
	40 ± 10	0.40	16	7	current
25.5	143 ± 24	0.08	37	37	Gavazzi and Perola
	112 ± 29	0.18	15	4	Machalski and Condon
	40 ± 9	0.61	20	5	current
26.5	300 ± 75	0.08	16	16	Gavazzi and Perola
	150 ± 27	0.31	30	1	Machalski and Condon

Secondly, an increase in size with radio power is not evident in our sample. However, this may be caused by the fact that the sources in our sample which have higher radio powers, are on average at higher redshift as well.

From the above, it is clear that it is necessary to separate the possible dependences of linear size on redshift from that of radio power. To this end, we have included the high resolution structural VLA data from a complete sample of radio galaxies from the GB and GB2 surveys (Machalski and Condon; 1985), which provides information at redshifts comparable to our sample, but which contains sources with higher radio luminosities. As in our sample, the subsample of Machalski and Condon contains a proportion of radio galaxies for which no spectroscopic redshift was measured. In these cases, photometric redshifts were calculated by Machalski and Condon, using the same absolute magnitudes and K-corrections, as used for our sample. In our analysis we have included from their sample only the radio galaxies with $z < 0.4$, in order to avoid large effects due to errors in the determination of magnitudes close to the PSS plate limit.

The median linear size for 1 decade intervals in radio power, and the median redshift in the interval were calculated for each of the three samples. The results are given in Table 3. The highest values of $D^{\rm med}$ are found locally at high $\log P$, the smallest at high z and at low $\log P$.

By comparing the value of the median size at each radiopower – using the values from Gavazzi and Perola as a zero point – we can take out any dependence of the median linear size on radio luminosity. Figure 8 shows the linear size of the sources in our subsample and those from Machalski and Condon vs redshift for two intervals in radio power. A large circle in each figure shows the median size from Gavazzi and Perola. Figure 9a shows the median size at each radiopower, normalized to the "local" median value *at the same radio power*, vs redshift. Both show a definite decrease of median linear size with increasing redshift.

In addition, Fig. 9a shows, that galaxies of different radio luminosities show essentially the same z-dependence. This indicates that the correlation between size and radio power, seen in the local sample, must be present at higher redshifts as well.

We can test this by this time taking out an assumed size redshift relation from the data. Using a simple powerlaw best fit to the points in Fig. 9a, we have transformed the median size found at each redshift to its value at the redshift of the local sample (0.08). The median sizes thus found show a dispersion of less than 10% at each radio power, indicating that the size radio power relation is very similar at every redshift. The median linear size vs radio power found by combining the medians from the three samples is given in Figure 9b.

We may conclude, that there is evidence for both a relation between size and redshift, and between size and radio power at redshifts $z < 0.75$. The correlations are not induced, because they result from independent surveys. Only the combination of these high resolution surveys, with different ranges in redshift and radio power, make a direct determination of these relations possible. Although the physical meaning is not clear, and the samples used are still relatively small, for the *red elliptical radio galaxies* we may provisionally adopt the following relations:

$$D(z) \propto (1+z)^{-3.0}, \quad \log P \in [23.0, 27.0]$$

and

$$D(P) \propto P^{0.31}, \quad z \in [0.08, 0.61]$$

The consistency between the sizes in our sample and those in the sample of Machalski and Condon, again indicates that we have not consistently underestimated the angular sizes of the sources in our subsample in any significant way. The fact that we do not have complete spectroscopic redshift information on the objects in our sample, may introduce some smearing of the relations, but this will not seriously influence the value of the median, because medians tend to be insensitive to the exact shape of a distribution.

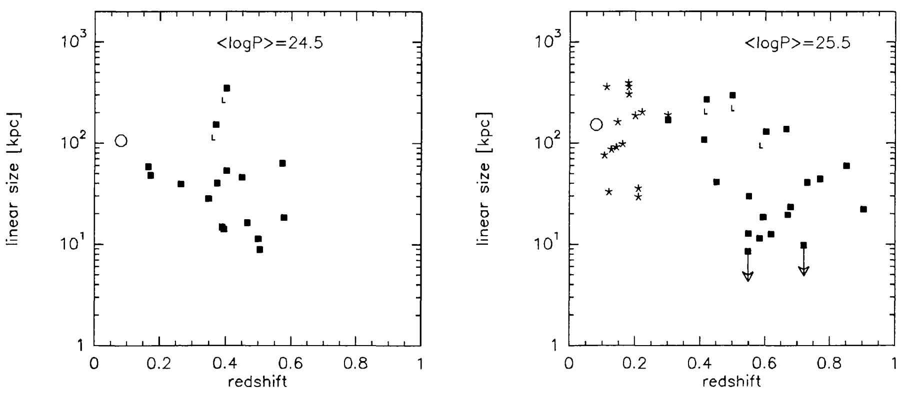

Fig. 8. Linear size versus redshift for the *red radio galaxies* for two intervals in radio power: $24 < \log P < 25$, and $25 < \log P < 26$. The large, open circles are the median values of Gavazzi and Perola. Asterisks are sizes from Machalski and Condon. Filled squares are sources from the current sample. If a source is accompanied by an "L", the angular size was taken from the LBDS source list

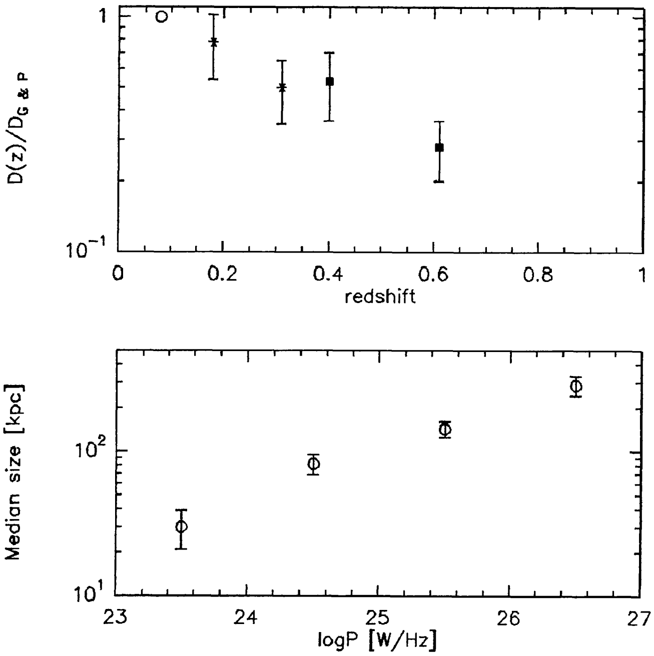

Fig. 9. **a** The ratio of median linear size of red radio galaxies from the current sample, or from the sample of Machalski and Condon in an interval of radio power, and the median value of the "local" sample at the same radio power. Filled squares are data from the current sample. Asterisks are data from Machalski and Condon. **b** The median linear size vs radio power, found by first transforming the medians at higher redshifts to their values at $z = 0.08$, and then combining the resulting value with the median size from Gavazzi and Perola

6. Conclusions

1) The median angular size of radio sources decreases considerably at low flux densities. At 3 mJy it is as low as 2″. This is largely due to the emergence of the "blue" radio galaxy class.

2) The purely optical distinction made between red and blue radio galaxies manifests itself in a difference in radio-morphology as well. Blue galaxies are for the most part unresolved at 1″ resolution, while red galaxies almost never are. The resolved and extended blue galaxies may represent different sub-populations or different stages in evolution.

3) Using spectroscopic and photometric redshifts, we have studied a number of intrinsic morphological properties of the *red radio galaxy* population. The radio emission of these objects is – with a few exceptions not very extended and seldom exceeds 100 kpc. We have found definite evidence for a relation between linear size and *redshift*. Moreover, the relation between size and *radio power*, found by Gavazzi and Perola (1978) for red radio galaxies with $z < 0.1$, is found to be present at higher redshifts as well, and is similar in form to the relation seen locally.

4) High resolution observations of LBDS radio sources are a very powerful aid for deep optical identifications. From a comparison with the optical identifications by Windhorst et al. (1985), we have shown that the contamination fraction is dependent on optical type. For the red galaxies 97% of the claimed identifications is correct, for the blue galaxies 84%. For the total sample the reliability is 91%, which is consistent with Windhorst et al.

The morphological analysis of the several radio galaxy populations needs further investigation. It should be extended to even lower flux densities. Deep optical identifications based on the VLA radio positions in several colors should be made and, wherever possible, redshifts should be measured in order to obtain a complete picture. Work on all these subjects is in progress.

Acknowledgements. We would like to thank all the staff at the VLA for their helpfulness and hospitality during our two visits there. MJAO acknowledges ASTRON/ZWO for financial support (grant 782-373-009). The Leiden computer group was very helpful when reduction problems arose. We also thank Wim Brokaar and Robert Haas for making the photographs. The referee of this paper has given us some very useful suggestions, which have enabled us to clarify some points in our discussion. The National Radio Astronomy Observatory is operated by Associated Universities Inc., under contract with the U.S. National Science Foundation.

Appendix

An empirical determination of the statistical errors associated with the VLA positions and flux densities

A functional form is adopted to describe the position and flux error distribution. The coefficients are determined empirically. For the position errors, we have used the following relations:

$$\sigma_{\alpha,\delta} = \sqrt{C_p^2 [RN/S_p]^2 + C_{\alpha,\delta}^2} \tag{A1}$$

and

$$\sigma^2 = \sigma_{\alpha,\delta}^2 + C_{\text{optical}}^2 \tag{A2}$$

The first term is a signal-to-noise (S_p/N) dependent coefficient. The error circle radius is proportional to R, the number of uncorrelated beam areas covered by the source. The second term is the absolute calibration error in the radio position.

Starting with the 85 sources with a possible identification, one can iteratively calculate C_p and $C_{\alpha,\delta}$ from an optical – VLA position comparison. In each iteration, the average position difference and standard deviation was calculated for α and δ separately and offsets larger than 2.5σ were flagged for the next iteration. This was continued until a stable situation was reached. C_{optical} was taken to be 0″.5 in both directions (Windhorst et al., 1984b).

Any systematic offset between the VLA- and optical position frame was found to be negligible (<0″.1). Therefore, we have rather arbitrarily set $C_\alpha = C_\delta = 0''.05$. The value of C_p is found to be 0″.62 = 0.45 HPBW, which is consistent with what is found at lower resolution. Errors given in Table 1 were calculated using the above values. Figure 10 shows the absolute (a) and normalized (b) error distribution. About 30% of the sources show optical-VLA radio position differences in excess of 1σ, showing that our choice of the values for the error parameters is indeed correct.

For the determination of the error in the total flux, a similar function was used:

$$\sigma_S^{\text{VLA}} = S^{\text{tot}} \sqrt{[N/S_p]^2 + F_0^2} \tag{A3}$$

VLA fluxes transformed to 1412 MHZ were compared with the WSRT fluxes from the LBDS with their known errors. The parameter F_0 is again determined empirically. Because of the tenfold increase in resolution between the VLA and WSRT observations, diffuse flux can influence the determination of F_0. For this reason we have used only the 52 unresolved sources in our sample. Sources with more than 3σ deviations were assumed to

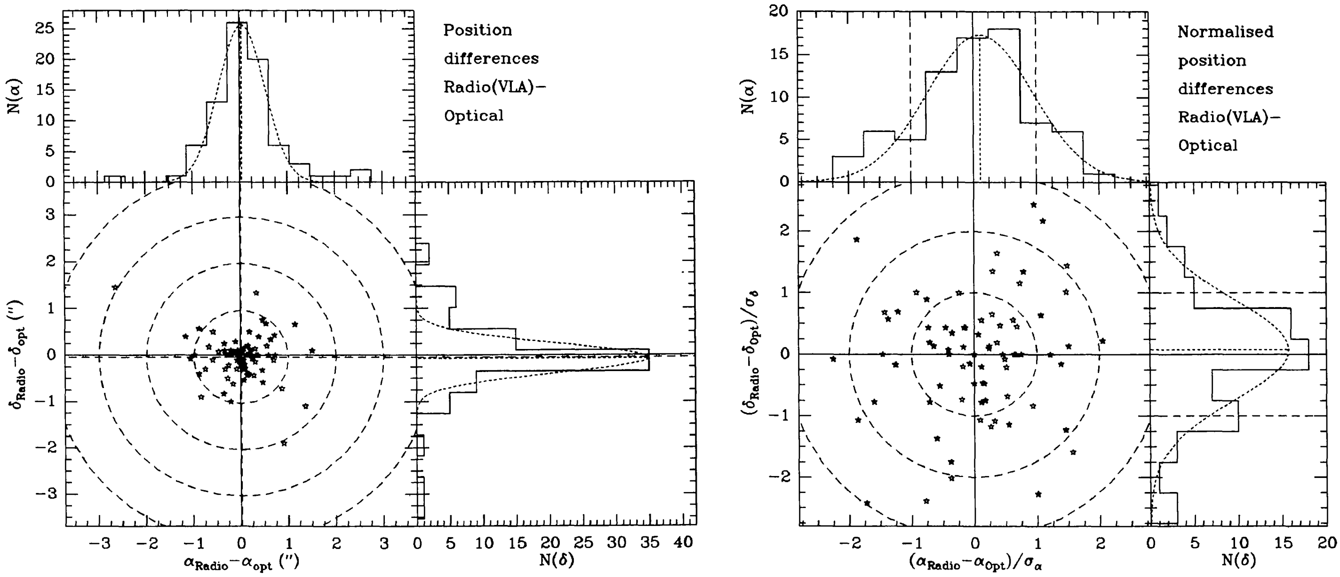

Fig. 10. **a** Absolute and **b** normalized VLA-optical position difference distributions

be variable and were ignored. Figure 11 shows the direct comparison of VLA and WSRT total fluxes.

The best value for F_0 found was 4.5% which includes a dispersion in 1412–1490 spectral index. In contrast with the position errors, a deviation of the average flux difference from zero was found, which corresponds to roughly a weighted average scale factor of $2\frac{1}{2}\%$. VLA fluxes are apparently consistently underestimated with respect to the WSRT flux. In absolute terms, however, this difference is small, maximally 5% for low signal-to-noise sources, and much less for strong sources. It is likely, but not certain, that this is caused by the uncertainty in the flux of 3C 286 at high resolution. Because the effect is small, we have *not* applied a correction factor. It should be noted that the effect is probably not caused by systematic errors in the assumed spectral indices. For reasonable values of α_{21}^{50} these can be no more than 1%.

Figure 12 shows the flux error distribution of the whole sample as well as the unresolved and resolved sources separately. The

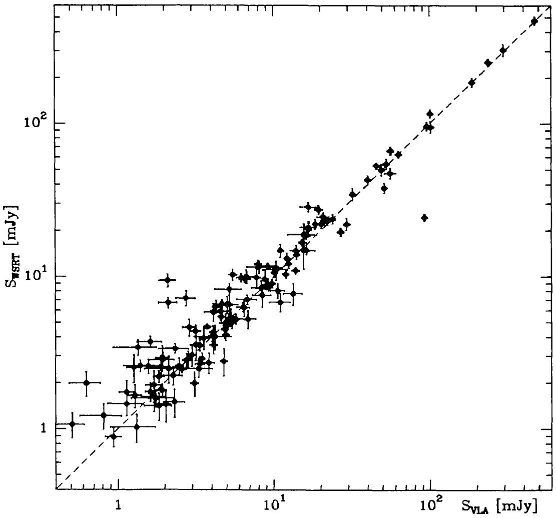

Fig. 11. Westerbork (LBDS) versus VLA total fluxes with their respective errors

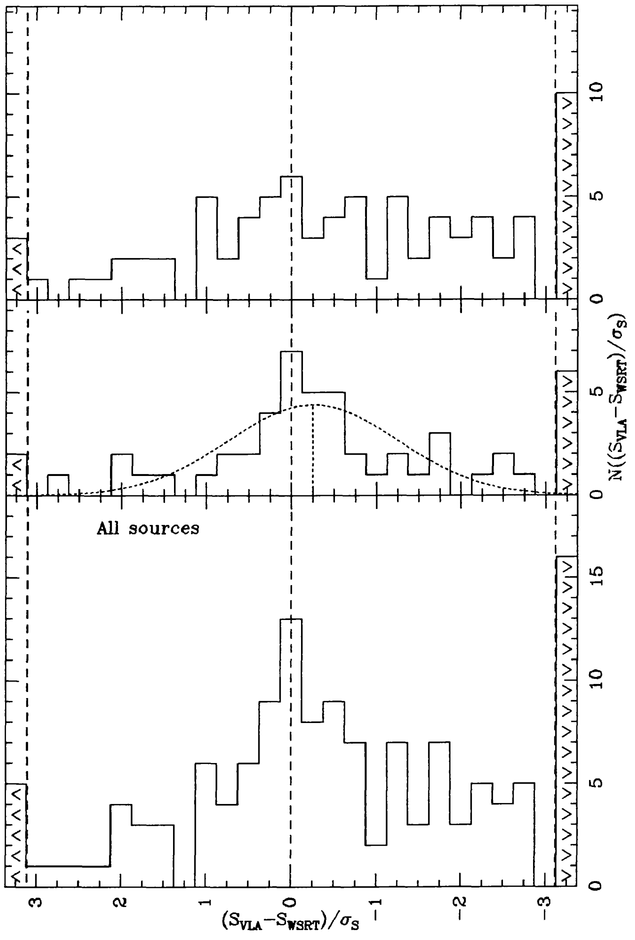

Fig. 12. The normalized flux error distribution of the total VLA sample (bottom), the unresolved sources only (middle), and resolved and extended sources only (top). The dashed curve in the middle graph is a Guassian best fit for the flux differences of the unresolved sources

Fig. 13. Contour plots of a number of sources in the VLA sample. Map sizes are multiples of 15″ × 15″. The lowest contour is 2.5σ. Crosses indicate the position of the optical counterpart

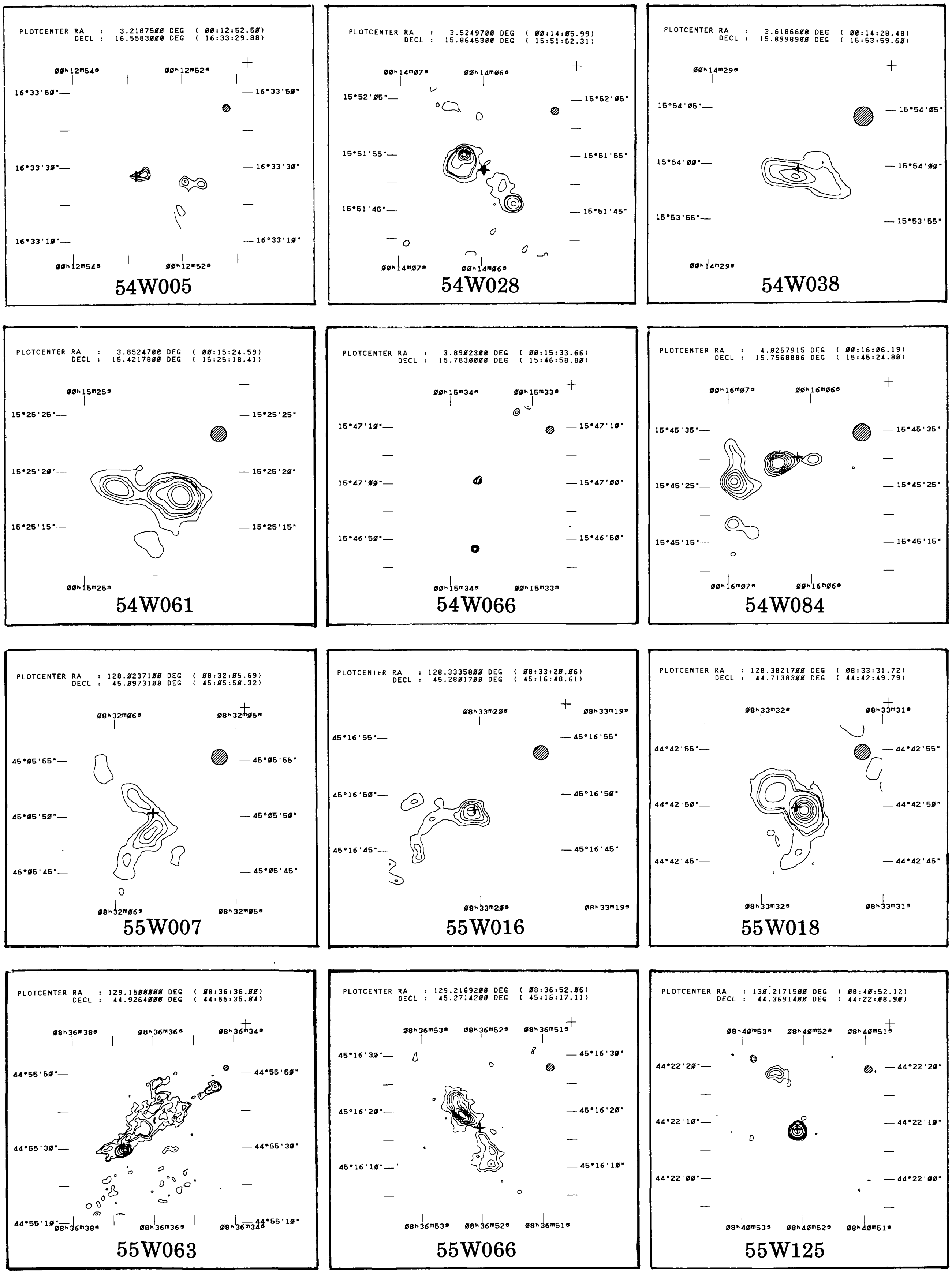

Fig. 13 (continued)

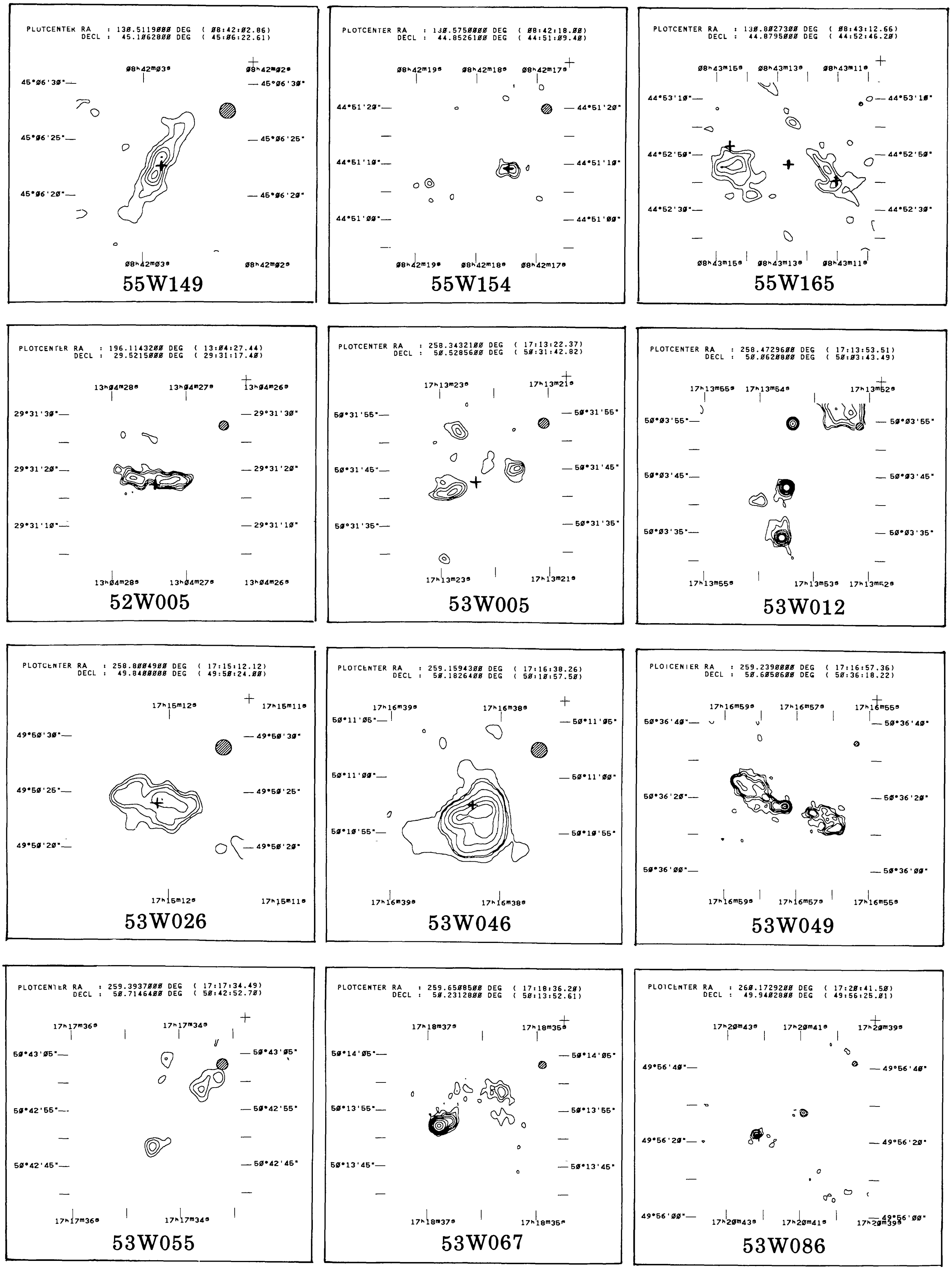

distribution of the resolved and extended sources is asymmetrical, indicating that a significant number of sources have diffuse, low surface-brightness halos, which were resolved out in the VLA maps. This is a factor which should be taken into account when making a comparative analysis.

References

Baars, J.W.M., Genzel, R., Pauliny-Toth, I.I.K., Witzel, A.: 1977, *Astron. Astrophys.* **61**, 99

Coleman, P.H., Condon, J.J.: 1985, *Astron. J.* **90**, 1431

Condon, J.J.: 1984, *Astrophys. J.* **287**, 461

Fielden, J., Downes, A.J.B., Allington-Smith, J.R., Benn, C.R., Longair, M.S. and Perryman, M.A.C.: 1983, *Monthly Notices Roy. Astron. Soc.* **204**, 289

Gavazzi, G., Perola, G.G.: 1978, *Astron. Astrophys.* **66**, 407

Kapahi, V.K.: 1975, *Monthly Notices Roy. Astron. Soc.* **172**, 513

Kapahi, V.K.: 1986, Highlights of Astronomy (ed. J.P. Swings) p. 371

Katgert-Merkelijn, J.K., Robertson, J.G., Windhorst, R.A. and Katgert, P.: 1985, *Astron Astrophys. Suppl.* **61**, 517

Kron, R.G., Koo, D.C., Windhorst, R.A.: 1985, *Astron. Astrophys.* **146**, 38

van der Laan, H., Katgert, P., Oort, M.J.A.: 1985, Proc Trieste Symp *Structure and Evolution of Active Galactic Nuclei*, eds. G. Giuricin, F. Mardirossian, M. Mezzetti, M. Ramella, Reidel, Dordrecht, p. 437

Lawrence, C.R., Bennet, C.L., Hewitt, J.N., Burke, B.F.: 1984, *Astrophys. J.* **278**, L95

Machalski, J., Condon, J.J.: 1985, *Astron. J.* **90**, 973

Meurs, E.J.A.: 1982, Ph. D. Thesis University of Leiden

Oort, M.J.A., Windhorst, R.A.: 1985, *Astron. Astrophys.* **145**, 405

Thompson, A.R., Clark, B.G., Wade, C.N., Napier, P.J.: 1980, *Astrophys. J. Suppl.* **44**, 151

Windhorst, R.A., van Heerde, G.M., Katgert, P.: 1984, *Astron. Astrophys. Suppl.* **58**, 1

Windhorst, R.A., Dressler, A., Koo, D.C.: 1986, in *IAU Symposium No* **124** on *Observational Cosmology*, eds. G. Burbidge, L.Z. Fang, Reidel, Dordrecht, (in press)

Windhorst, R.A., Kron, R.G., Koo, D.C.: 1984b *Astron. Astrophys. Suppl.* **58**, 39

Windhorst, R.A., Miley, G.K., Owen, F.N., Kron, R.G., Koo, D.C.: 1985 *Astrophys. J.* **289**, 494

Windhorst, R.A., Oppe, J.: 1986, (in preparation)